atures is involved during the impulsive phase, and single temperature analysis is inadequate, given the improvements in the observations. Multi-thermal analysis techniques, however, are limited in the detail with which the temperature distribution can be determined, even with more accurate observations.

5.3 THE ENERGETICS OF THE GRADUAL PHASE

K.T. Strong, R.D. Bentley, P.L. Bornmann, M.E. Bruner, P.J. Cargill, J.G. Doyle, J.R. Lemen, R. Pallavicini, G. Peres, S. Serio, G.M. Simnett, J. Sylwester, and N.J. Veck

5.3.1 Introduction

The gradual phase of a flare is best characterized by the smooth rise and decay of the soft X-rays (see Figure 5A.2). Just from inspection of the soft X-ray light curves of some typical flares, it is evident that the gradual phase comprises several different stages. During the rise of the X-ray emission, a completely different energy budget from that of the decay will be produced. Many flares show multiple peaks in their light curves, indicating that energy is released after the initial burst. The location of any such secondary energy release will also profoundly affect the relative importance of the terms in the energy budget of the flare.

The soft X-ray emission produced by the higher-temperature ($> 10^7$ K) plasma rises and decays more rapidly and peaks earlier than that produced by the cooler plasma (10^6 – 10^7 K). The impulsive phase usually occurs during the rise of the soft X-ray emission but there is no clear evidence of an impulsive component in the soft X-ray signal. Hence, in an energetics study the important question arises of what, if any, is the link between the impulsive and gradual phases.

We have avoided using the term "thermal phase" because it is misleading; a number of non-thermal energetics terms are associated with the gradual phase. The mass motions are an example; it is not clear whether they are peculiar to the early stages of a flare or whether they are also present later in the flare, which seems to be likely, as mass motions have been detected even in quiescent active regions (Acton *et al.*, 1981). We therefore attempted to evaluate the non-thermal terms as well as the thermal energy throughout the gradual phase of the five prime flares.

As the flare observations made with SMM were not specifically designed to address the energetics problem, our choice of flares (see Appendix 5A) represents a compromise. We identified a number of different "types" of flares that, although sharing the same physical processes, had somewhat different physical characteristics.

The Skylab Solar Flares Workshop (Sturrock 1980a) laid the foundations for the methodology used in this section, and we compare our results with those in the chapter by Moore *et al.* (1980), who reached five main conclusions about the gradual phase:

- the typical density of the soft X-ray emitting plasma is between 10^{11} and 10^{12} cm^{-3} for compact flares and between 10^{10} and 10^{11} cm^{-3} for a large-area flare;
- cooling is by conduction and radiation in roughly equal proportions;
- continual heating is needed in the decay phase of two-ribbon flares;
- continual heating is probably not needed in compact events;
- most of the soft-X-ray-emitting plasma results from "chromospheric evaporation".

Our goal was to reexamine these problems with the data from SMM and other supporting instruments as well as to take advantage of recent theoretical advances. SMM is capable of measuring coronal temperatures more accurately and with a better cadence than has been possible before. The SMM data set is also unique in that the complete transit of an active region was observed, with soft X-ray and UV images being taken every few minutes. We are therefore able to establish the pre-flare conditions of the region and see whether anything has changed as a result of the flare.

In the next subsection we describe the assumptions made in attempting to determine the required plasma parameters. The derived parameters for the five prime flares are presented, and the role of numerical simulations is discussed. Finally, we consider the overall implications of our results and discuss how both theory and observations have evolved since the Skylab workshop.

5.3.2 The Basic Physical Expressions

The quantities needed for this study are defined in terms of the fundamental plasma parameters of electron temperature (T_e), electron density (N_e), plasma volume (V), plasma velocity (v), and height (h). The four basic energies that we wish to obtain throughout the flares are the thermal energy (E_{th}) of the plasma,

$$E_{th} = 3\ N_e\ k\ T_e\ V \text{ ergs;} \qquad (5.3.1)$$

the kinetic energy (E_k) of the plasma,

$$E_k = 1/2\ M_p\ N_e\ V\ v^2 \text{ ergs;} \qquad (5.3.2)$$

the potential energy (E_p) of the coronal plasma,

$$E_p = M_p\ N_e\ V\ g_o\ h \text{ ergs} \qquad (5.3.3)$$

(where M_p is the proton mass and g_o is the gravitational acceleration at the solar surface); and the stored ionization energy in the plasma (E_i), which is the sum of the ioniza-

tion energy of every ion stage of all abundant elements existing up to the observed temperature. This latter component is dominated by the ionization energy of hydrogen and helium. Note that these energetics terms only apply in the above form for an isothermal plasma. However, the SMM data indicate that the coronal plasma during a flare is multi-thermal, and the integral forms of these equations must often be used (Section 5.3.2.1).

The energy flux terms and their corresponding timescales are as important as the individual energy terms for understanding the energy budget. There are three main terms: the conductive flux (F_c), which, in terms of the classical Spitzer-Harm theory of heat conduction, can be expressed as

$$F_c = -\kappa T_e^{5/2} dT_e/dh \text{ ergs cm}^{-2} \text{ s}^{-1}; \quad (5.3.4)$$

the radiative flux (F_r),

$$F_r = -A^{-1} \int N_e^2 P_r dV \text{ ergs cm}^{-2} \text{ s}^{-1}; \quad (5.3.5)$$

and the enthalpy flux (F_e),

$$F_e = (5/2A) K T_e d(N_e V)/dt \text{ ergs cm}^{-2} \text{ s}^{-1}. \quad (5.3.6)$$

The corresponding decay timescales (in s) are

$$\tau_c = 2 \times 10^{-10} N_e L^2 T_e^{5/2} \quad (5.3.7)$$

$$\tau_r = 10^7 T_e/N_e \quad (5.3.8)$$

$$\tau_e = 1.2 N_e(dN_e/dt)^{-1}. \quad (5.3.9)$$

It should be possible to derive all these quantities as a function of time throughout the flare from a knowledge of the plasma parameters and the geometry of the flaring loop. However, these quantities are not available directly from observations although the temperature and density can be inferred from soft X-ray line ratios. Generally, we derive the emission measure (N_e^2 V) from optically-thin line intensities. The SMM X-ray data can be used to derive the DEM. The temperature range available was 2×10^6 to 10^8K, but no information was available in one of the most interesting temperature domains, namely 2×10^5 to 2×10^6 K. There is considerable uncertainty in the quantities needed to derive these energetics terms, especially the density. However, for the five prime flares, the values obtained for each of these energetics terms are discussed.

5.3.2.1 Multi-thermal Modeling

Several quantities are discussed above which express the energy content of the various flare components with the assumption of an isothermal plasma. However, there is strong evidence from SMM data that the coronal plasma is multi-thermal during flares (Figure 5.3.1). For this reason, an attempt was made to model the temperature distribution of the flare plasma from spectroscopic data obtained with various SMM instruments. In this section we present the multithermal forms of the expressions for the thermal energy (E_{th}) and radiative flux (F_r) and discuss the techniques which were used to derive the temperature distribution of the plasma. The temperature distribution of the plasma may be characterized by the differential emission measure (DEM), q(T), which is defined as

$$q(T)\, dT = N_e^2\, dV. \quad (5.3.10)$$

With a multithermal assumption, several of the quantities given in Section 5.3.2 are modified: the expression for the radiative flux becomes

$$F_r = \int P_r(T) q(T) dT \text{ ergs s}^{-1}, \quad (5.3.11)$$

where $P_r(T)$ is the radiative power loss function; the thermal energy, dE_{th}, of a volume element dV with temperature T and density N_e is given by

$$dE_{th} = 3 N_e k T_d V \text{ ergs}. \quad (5.3.12)$$

If the density within the volume, V, is assumed to be uniform, Equation 5.3.12 may be integrated to yield

$$E_{th} = \frac{3kV^{1/2} \int Tq(T)dT}{(\int q(T)dT)^{1/2}} \text{ ergs}. \quad (5.3.13)$$

Alternatively, if the pressure, p = nT, within the volume is assumed to be uniform, the thermal energy becomes,

$$E_{th} = 3_k V^{1/2} [\int T^2 q(T)\, dT]^{1/2} \text{ ergs}. \quad (5.3.14)$$

The DEM was derived for the soft X-ray emitting thermal plasma by two different methods. The first method was an inversion technique initially developed by Withbroe (1976) and extended by Sylwester *et al.* (1980, 1984). This method has been applied to the five prime flares in this study by using data from four BCS lines and the six HXIS energy bands.

The four lines observed by BCS consist of the helium-like resonance line ($^1S_0$–$^1P_1$) in Ca XIX and Fe XXV and the lithium-like satellite line k in Ca XVIII ($^2P_{1/2}$–$^2D_{3/2}$) and j in Fe XXIV ($^2P_{3/2}$–$^2D_{5/2}$). These satellite lines are dielectronically populated and so their intensity ratios relative to the resonance lines are temperature sensitive and independent of ionization balance. The effects of blending with nearby lines were removed by fitting a fully synthesized spectrum to the data.

The HXIS coarse field-of-view data were analyzed by summing over the whole flare area rather than by studying individual pixels or groups of pixels, because it covers an

area comparable with that of the BCS collimator (6 arc min FWHM). This approach probably does not affect estimates of the overall energy budget of the flare but it could possibly mask secondary energy releases at other sites away from the original flare location.

Any particular solution of q(T) is probably not unique. However, various tests were performed which showed that different but acceptable, solutions for q(T) generally conserved the total emission measure, $\int q(T)dT = \int N_e^2 dV$. A further limitation arises from the fact that BCS and HXIS are insensitive to emission from plasmas with temperatures below about 10^7K, although a considerable amount of thermal energy is expected to be contained in these plasmas. Both of these problems could be lessened by including softer X-ray or UV data, which would extend the results to lower temperatures and thus better constrain the range of acceptable solutions for the DEM. The lowest energy FCS channels are sensitive down to 2×10^6K. However, since the cadence of the FCS observations was typically about 300 s per image, the FCS data were included for only one flare; 1980 August 31 double flare.

A second method for determining the DEM which combines data from BCS, HXIS, and HXRBS, has been developed by Bely-Dubau *et al.* (1984). In contrast to the approach just described, this method assumes a parametric description for the DEM. The parameters are adjusted until an acceptable agreement with the observations is achieved. So far, this method has only been applied to the 1980 June 29 flare. This technique is not subject to the problems which arise with an inversion technique when the emission functions cover a large proportion of the temperature range of the model. Eight BCS lines (the Ca XIX w, q, and k lines, Fe XXV w, q, and j lines, and Fe XXV r and s lines), the six HXIS energy bands, and the eight lowest energy HXRBS channels are included in the model. The model includes thermal and non-thermal components, and thus an important factor for energetics studies is the lower-energy cut-off for the nonthermal spectrum. Bely-Dubau *et al.* (1984) found that any cutoff value between 15 and 25 keV gave an acceptable fit to the data, but resulted in a considerable variation in the estimates for the energy budget of the flare.

Bornmann (1985a,b) has developed a new method for estimating the temperature and emission measure during the decay of the gradual phase from the shape of the light curves of soft X-ray lines. The rates at which the observed line fluxes decayed were not constant. For all but the highest temperature lines observed, the rate changed abruptly, causing the fluxes to fall at a more rapid rate later in the flare decay. These changes occurred at earlier times for lines formed at higher temperatures. Bornmann proposed that this behavior was due to the decreasing temperature of the flare plasma tracking the rise and subsequent fall of each line emissivity function. This explanation was used to empirically model the observed light curves and to estimate the temperature and the change in emission measure of the plasma as a function of time during the decay phase of the 1980 November 5 flare. This method provides a simple and independent measure of the temperature and cooling rate during the decay of the flare.

5.3.3 The Prime Flares

A more detailed description of the prime flares and a list of publications discussing their relevant aspects are given in Appendix 5A. In keeping with the impulsive phase section, we have emphasized the 1980 April 8 flare, but a brief discussion of the other prime events is given below.

5.3.3.1 The 1980 April 8 Flare

The M4 flare of 1980 April 8 originated in a small, isolated, bipolar region that was part of a delta configuration in NOAA active region 2372. The flare had an optical importance of 1B and showed multiple impulsive spikes in the HXRBS light curve, the brightest occurring at 03:05 UT. For details see Appendix 5A.

Both BCS and FCS showed that until 10 min before the flare, the level of coronal emission from the whole region was declining (25% in Ca XIX and about a factor of 2-3 in O VIII). The coronal temperature also appeared to be slowly dropping, changing from about 2.5×10^6 to less than 2×10^6K during the interval from 00:50 UT to 02:59 UT. At about 02:50 UT, the BCS Ca XIX lines started to increase in intensity. At 02:54 UT, the density measured with UVSP at the eastern footpoint began to rise exponentially, reaching a value of about 3×10^{12} cm^{-3} at 03:02 UT, when the measurement sequence was terminated. Both intensity and density were still rapidly increasing at this time, so that considerably larger values could have been reached at the time of the peak emission. Machado (1980) has identified the eastern footpoint with the isolated bipolar region discussed above. The electron density, as derived from the P78-1 O VII line ratios, reached its maximum of 10^{12} cm^{-3} at 03:05 UT, before any of the soft X-ray intensities had peaked. Since the characteristic temperatures of the two determinations differ by an order of magnitude, the fact that the derived densities are comparable suggests that the two regions were not in pressure equilibrium with each other and implies the existence of temperature gradients across the magnetic field. This result must be treated with caution, however, since the two determinations were not made simultaneously.

Subsequent development of the flare first involved the leader spot, via loops connecting it to the intermediate bipolar region, after which it spread to the trailer spot. Later in the gradual phase, the region of soft X-ray emission expanded southward. The HXIS images show that at least three discrete sources were involved during the rise phase, suggesting the existence of at least two flaring loops. A description of the magnetic field structure can be found in Chapter 1 of these proceedings.

The observations were analyzed along the lines discussed in Section 5.2.3. The HXRBS data can be represented by either a thermal or a power law spectral form. For analysis of the microwave data from Toyokawa, temperatures determined from fits to the thermal form of the HXRBS spectra were used to characterize the electron source of the hard X-ray emission for selected intervals throughout each burst. Observations obtained at 3.75 GHz were in the optically thick portion of the microwave spectrum throughout the impulsive and gradual phases of the flare and therefore enabled the computation of an effective area. The 3/2 power of an effective area was taken as an estimate of the size of the emitting volume. The maximum turbulent velocity derived from the BCS spectra was 120 km s^{-1}, assuming a single temperature determined from spectral analysis and neglecting the source size (Antonucci *et al.*, 1982). The upflow was 200-300 km s^{-1}. Non-thermal line widths for the Fe XXV lines from P78-1 were derived by U. Feldman and S. Graham in work done specifically for this workshop. They assumed that the line profile was given by the convolution of three gaussians: one for the thermal width of the line, one for the turbulent velocity, and one for the angular size of the source. They assumed the angular size to be 30 arc sec and used the temperature value derived from P78-1 measurements of the j/w line ratio. Their results range from 100 to 300 km s^{-1}, bracketing the result of Antonucci *et al.* (1982).

We used the DEM distribution to represent the ensemble of soft X-ray observations of the gradual phase of the flare. We chose this approach because the DEM is proportional to both the observed intensities and the total radiated power, even in the presence of inhomogenities in the radiating atmosphere. Four computations (Figure 5.3.1) of the DEM were made, corresponding to the four FCS rasters. BCS and HXIS data were selected for the times when the flaring plasma was being scanned with FCS. This technique is particularly powerful in placing constraints on the DEM distribution. The use of several isolated spectral lines provides intensity measurements for which the contribution function is well known. The inclusion of the four broad-band measurements from HXIS ensures that no important radiative energy sources have been omitted and provides a constraint on the total emission. Each DEM distribution shows two peaks, one near 2×10^7K and the other near 4×10^6K. The high-temperature peak is seen to move toward lower temperatures as the flare cools, as one would expect.

The temperature curves (see Figure 5.3.2) should be interpreted as indicators of the slope of the electron energy distribution in the energy range appropriate to each instrument; they do not necessarily represent physically meaningful quantities. With the exception of the temperature derived from HXRBS, the other temperatures agree to within a factor of 2. Assuming these estimates are a measure of the plasma temperature, they are not misleading, provided that one does not attempt to extrapolate outside the relevant electron energy range. The higher values of the HXRBS temperature parameter show that the electron spectrum producing the hard X-rays is relatively flatter than that producing the emission observed with the other instruments.

Density measurements for this flare are available from several observational sources (Figure 5.3.3). At the time of the maximum at 03:05 UT, the O VII density is probably dominated by material in the footpoints and does not reflect the average density in the loop system, since the evaporation phase has just begun.

Three volume estimates for the April 8 flare have been made: (1) the observed size in the HXIS fine field of view; (2) the apparent area derived from hard X-ray and microwave fluxes, and (3) using observed X-ray line intensities. The first two methods involve simple assumptions about the geometry of the emitting region to estimate the volume from the apparent area, whereas the third uses the derived electron density to compute the effective volume from the observed emission measure. The two estimates based on apparent areas agree fairly well during the impulsive phase, whereas the volume calculated from derived density and emission measure estimates is lower by a factor of 100 to 1000 (Figure 5.3.4). Although some of this discrepancy may be due to errors in the atomic data or in the underlying assumptions, the differences are important and have been cited as primary evidence for the existence of a small filling factor. The volumes derived from all these methods converge during the gradual phase. This probably indicates evolution of the geometry of the plasma during the gradual phase, with the filling factor tending toward unity. The evaluation of the filling factor is of obvious importance to the question of energetics, since the thermal energy content of the plasma is directly proportional to the total volume.

Figure 5.3.5 shows emission measures as functions of time determined from the BCS and HXRBS spectra. The P78-1 results of Doschek *et al.* (1981) are comparable. The four circles indicate the emission measures determined from the combined analysis of FCS, BCS, and HXIS data and correspond in time to the four FCS rasters.

Values of P_r and E_{th} (Figure 5.3.6) were determined for the high-temperature component (10^7 to 5×10^7K) in a similar manner as for the 1980 June 29 flare (see below). The volume of 10^{27} cm^3 was estimated from HXIS fine-field-of-view images (Table 5.2.1). The peak value for E_{th} was found to be about 1.4×10^{30} ergs, which compares well with 9.4×10^{30} ergs for the total electron energy (Table 5.2.1). Note from Figure 5.3.1 that the low temperature component of the DEM is at least a factor of 10 larger than the high-temperature component which would mean that the thermal energy of the two components are approximately equivalent.

Figure 5.3.7 is the version of Figure 5.1.1 for this particular flare and shows the complete energy budget derived from the above physical quantities plotted. The kinetic energy in the upflows and in the turbulence was calculated using

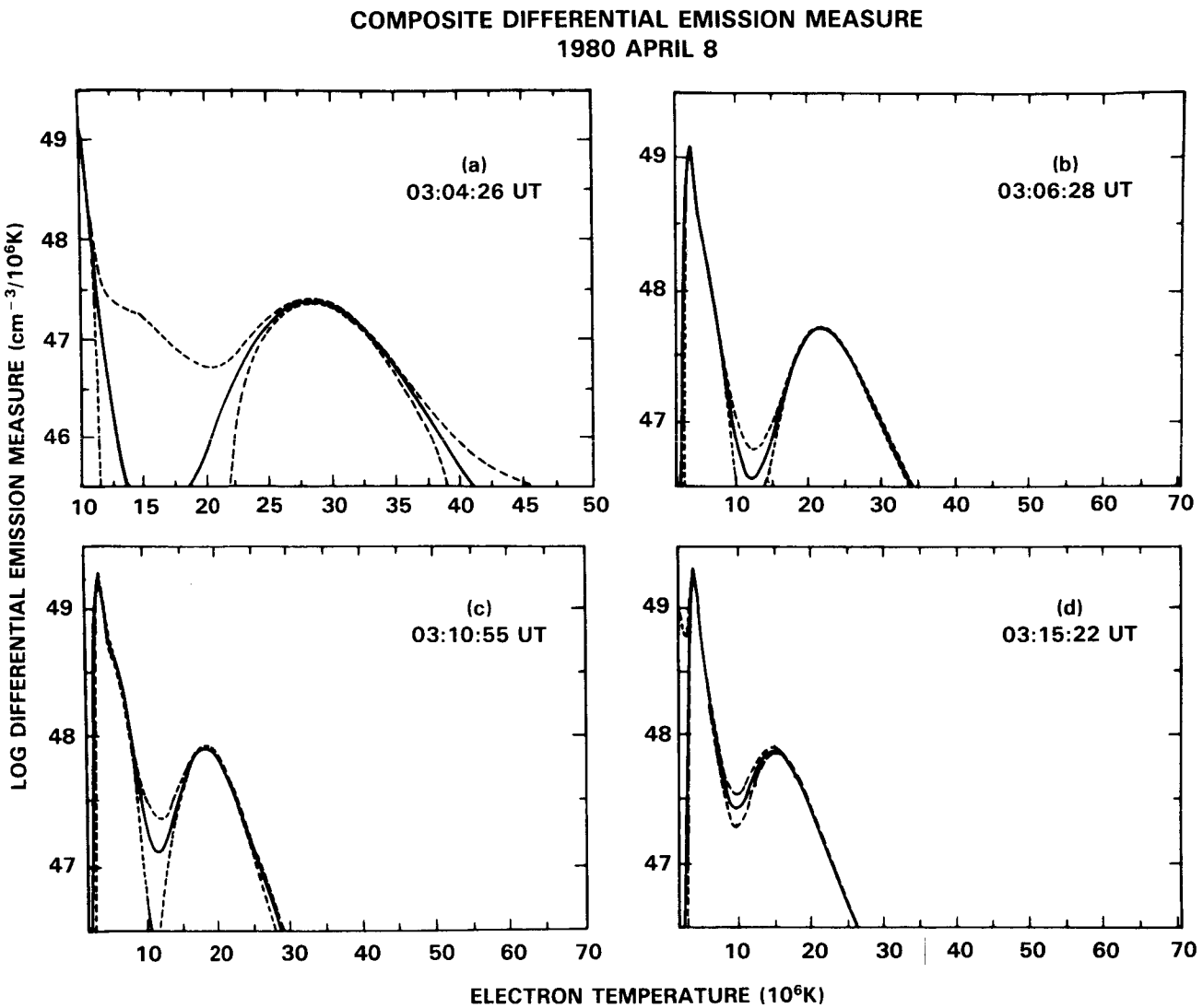

Figure 5.3.1 The DEM models calculated for four times during the 1980 April 8 flare. Note that, even during the rising portion of the gradual phase when the flare is at its hottest, there is a significant low temperature component. As the flare evolves the high temperature component of the DEM decays in temperature eventually merging with the low temperature component.

the P78-1 velocities and the BCS emission measures. The energy in the electrons determined from the thermal fit to the HXRBS spectra was used in Figure 5.3.7 rather than the thick-target non-thermal energy since the instantaneous energy in the electrons for that case is not significant. The gravitational potential energy and ionization energy are not plotted here, as they are too small to show on this scale. The peak gravitational energy is 3×10^{28} ergs.

Note that at 03:06 UT the total energy remains essentially constant. The slow drop in the total energy after this time (less than 30%) may be due to conductive losses which have not been included in the plot.

5.3.3.2 The 1980 May 21 Flare

This flare was chosen because it has exceptionally good data for the impulsive phase. However, the FCS and UVSP coverage during the gradual phase was very poor. They were in unsuitable modes during this event and so can contribute very little to the discussion of the energetics of the gradual phase, which is well described by Duijveman *et al.* (1983).

5.3.3.3 The 1980 June 29 Flare

This event occurred on the limb, and so the determination of the volume of the flare is different than for a disc

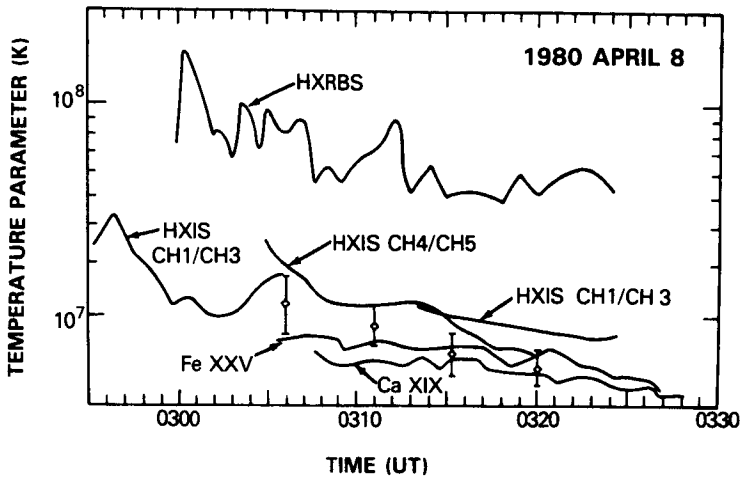

Figure 5.3.2 Evolution of the temperature parameter for 1980 April 8 derived from a number of different sources. The diamonds are derived from the high temperature component of the DEM calculations shown in Figure 5.3.1. The error bars represent the full width at half maximum of the distribution.

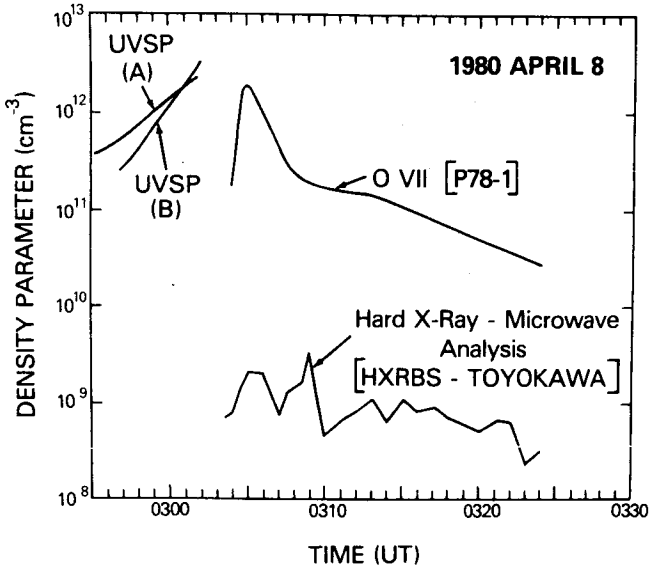

Figure 5.3.3 Evolution of the density parameter from UVSP Si IV/O IV line ratios and O VII measurements from P78-1, compared to the density derived from the hard X-ray—microwave analysis.

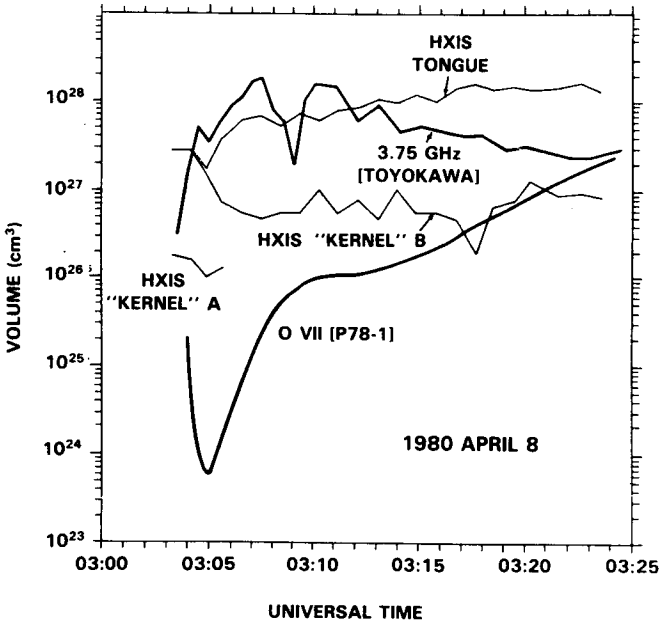

Figure 5.3.4 The history of the volume parameter from the 1980 April 8 flare from several different sources.

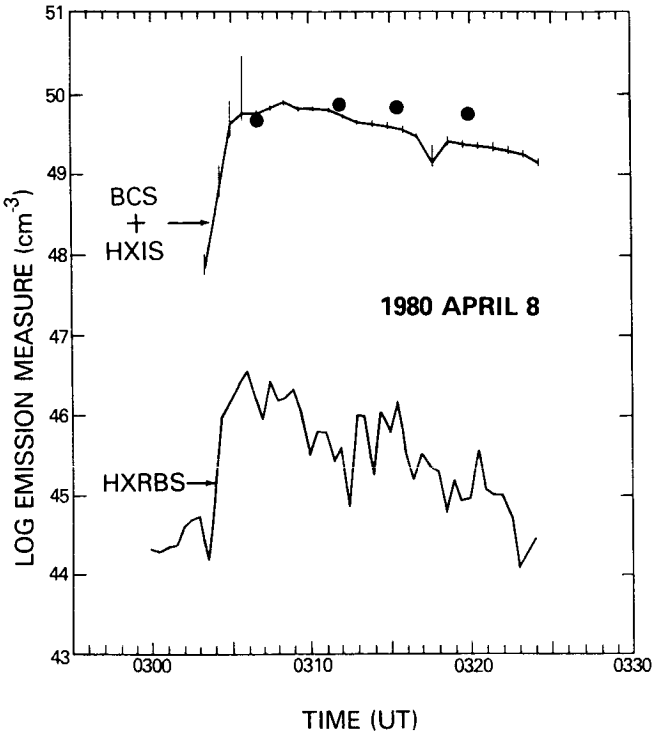

Figure 5.3.5 The evolution of the emission measure in the 1980 April 8 flare from the BCS, HXIS, and HXRBS data (thermal assumption). Note that the soft X-ray emission measure is over 3 orders of magnitude larger than that for the hard X-ray source. The BCS and HXIS value does not include information on the low temperature component ($< 10^7$K). The filled circles represent the emission measure calculated for temperature $> 2 \times 10^6$ K by including the FCS data with the BCS and HXIS observations. They show that the component between 2×10^6 K and 10^7 K is comparable to the component in the 10 to 20 $\times$ 10^6K range, at least later in the flare.

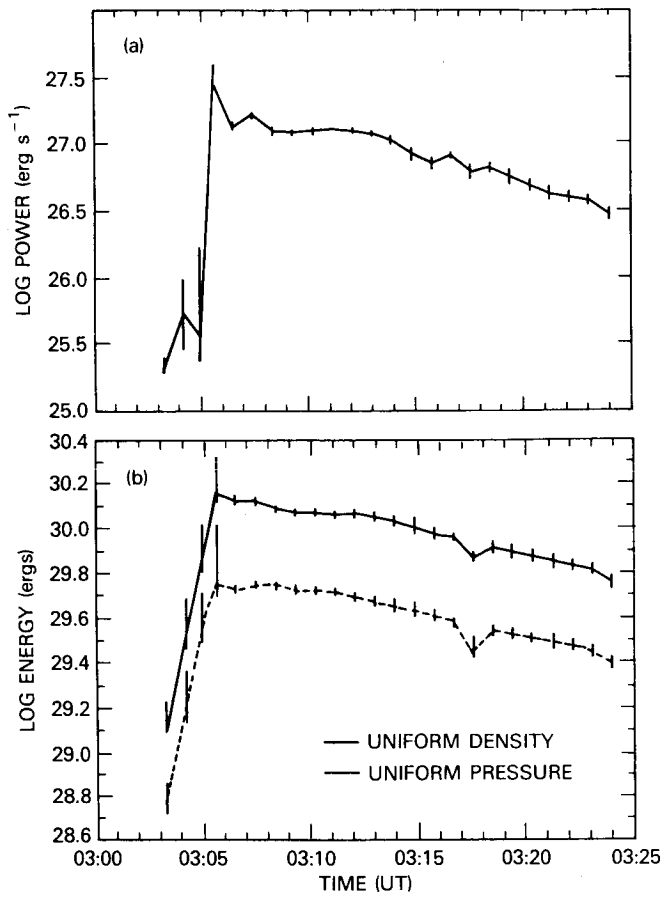

Figure 5.3.6 The evolution of (a) the radiated power (ergs s^{-1}) and (b) the thermal energy (ergs) for the 1980 April 8 flare from combined BCS and HXIS data. The error bars represent $\pm$ 1σ uncertainties. These quantities are calculated for the thermal plasma above 10^7 K only.

Table 5.3.1 Energetics of the 1980 June 29 Flare

Energetics term	BCS + HXIS	Ca XIX Fe XXV	Fe XXI O V	HXIS	HXRBS
Emission measure (cm^{-3})	2×10^{49}	3.5×10^{49} 5.6×10^{49}	7.9×10^{43} 0.32×10^{43}	3.3×10^{45}	9×10^{45}
Radiative power (ergs s^{-1})	8×10^{26}	2×10^{27}		2.3×10^{28}	
Integrated thermal energy (ergs)	2.8×10^{26}				
Radiated energy (ergs)	3.7×10^{29}				

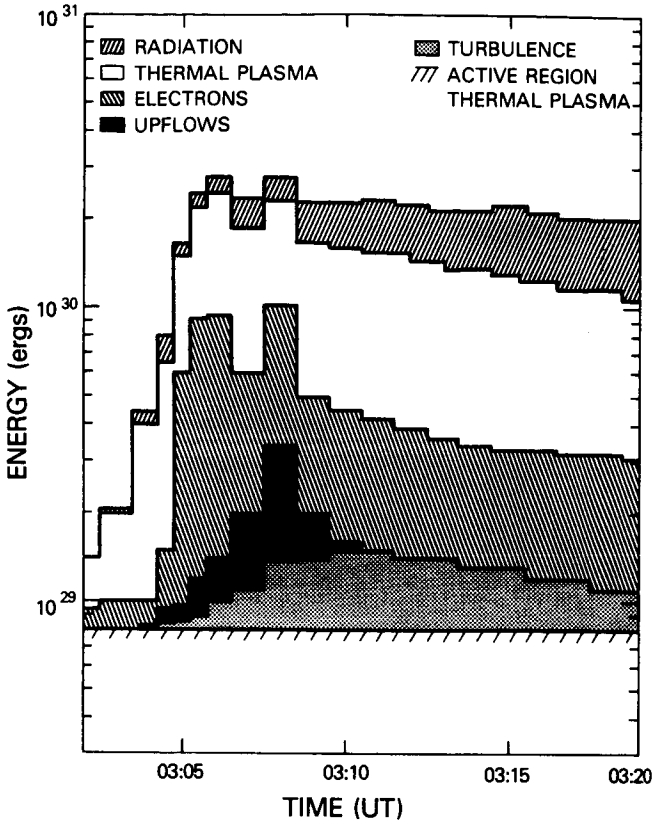

Figure 5.3.7 The distribution of the flare energy among various reservoirs and active phenomena as a function of time for the 1980 April 8 flare (c.f. Figure 5.1.1). The width of the histogram bins represents the time resolution for each of the parameters measured. Note that late in the flare (after 03:09 UT), the sum of the components remains effectively constant in spite of the fact that several of the components are varying.

flare. Although we have the height structure and hence the area of the flare, the line-of-sight depth is still unknown. Further, it seems that part of the flare was probably behind the limb. The FCS images were used to determine the area of the flare, which gave a value of 2×10^{19} cm^2. The microwave data imply an area of 3.3×10^{19} cm^2, although interferometric observations gave an area of an order of magnitude less.

Normally, one does not expect to find significant line shift in the BCS data for a limb event. However, this flare gave a velocity of 370 km s^{-1} at the flare onset. Turbulent velocities of about 200 km s^{-1} were estimated from the BCS Ca XIX line profiles. Vertical motions were measured by several instruments: 200 km s^{-1} in the lower corona, 500 km s^{-1} above 1.2 solar radii, and 1100 km s^{-1} from the type II burst.

A multi-thermal analysis of the high-temperature component of the flare plasma was made for this flare. For the determination of the DEM, the intensities of four lines observed by BCS and the integrated HXIS coarse-field-of-view fluxes were used. The DEM was then convolved with the radiative power loss function, $P_r(T)$, of Summers and McWhirter (1979) to give the total radiative loss rate results shown in Figure 5.3.8(a). Since $P_r(T)$ is approximately constant with temperature near 2×10^7K, the behavior of the radiative flux with time is similar to the behavior of the total emission measure with time. The value of E_{th} is shown in Figure 5.3.8(b), as calculated assuming either uniform pressure or uniform density throughout the volume of plasma with a given temperature. The volume was estimated to be 7×10^{26} cm^3 by assuming a density of 2×10^{11} cm^{-3}, which is typical of the estimated densities for the other principal flares we considered (see Table 5.2.4). The peak value of 7.8×10^{29} ergs for E_{th} calculated assuming uniform density is comparable to the total energy inferred (1.3×10^{30} ergs) for the non-thermal electrons above 25 keV. The turbulent energy derived from the BCS line widths was discussed in Section 5.2.3.4. The peak turbulent energy observed during the impulsive phase was approximately 3×10^{28} ergs.

There was a mass ejection during the 1980 June 29 event (Wu *et al.*, 1983). The maximum temperature (2×10^6K) and density (4×10^{11} cm^{-3}) derived from the XRP data, together with an assumed velocity, were used to simulate the mass ejection using an MHD model (Wu *et al.*, 1983). The simulation produced spatially wide, large-amplitude, temporally steepened MHD waves but no shocks. This result seems to be supported by the fact that a type II radio burst was observed late in the event for only a few minutes. The density enhancements moved away from the Sun at the same velocity (1000 km s^{-1}) as determined with the Mauna Loa K-coronameter. However, the observation of the coronal transient included a rarefaction that does not appear in the simulation. The model enables us to derive the energy associated with the transient; the quantities are: peak temperature, 16.5×10^6K; peak density, 3.0×10^{10} cm^{-3}; total volume, 1.0×10^{27} cm^3; and total energy, 4.0×10^{33} ergs. Comparison with the observed pB (polarization $\times$ brightness) signal, derived from C/P data to be 7×10^{-8}, gave a result that was a factor of 3 too high. This implies that the magnitude of the calculated density enhancement was high by at least 50% in the closed-field case and a factor of 3 higher in the open-field case. The peak values of the energetics terms of this flare are listed in Table 5.3.1, in which only part of the radiative energy could be estimated based on the available data. The computed total energy included all the energy sources (i.e. magnetic, potential, kinetic and thermal).

Using the alternative technique of Bely-Dubau *et al.*, (1984) described above (Section 5.3.2.1), we find the energy content as a function of time given in Table 5.3.2.

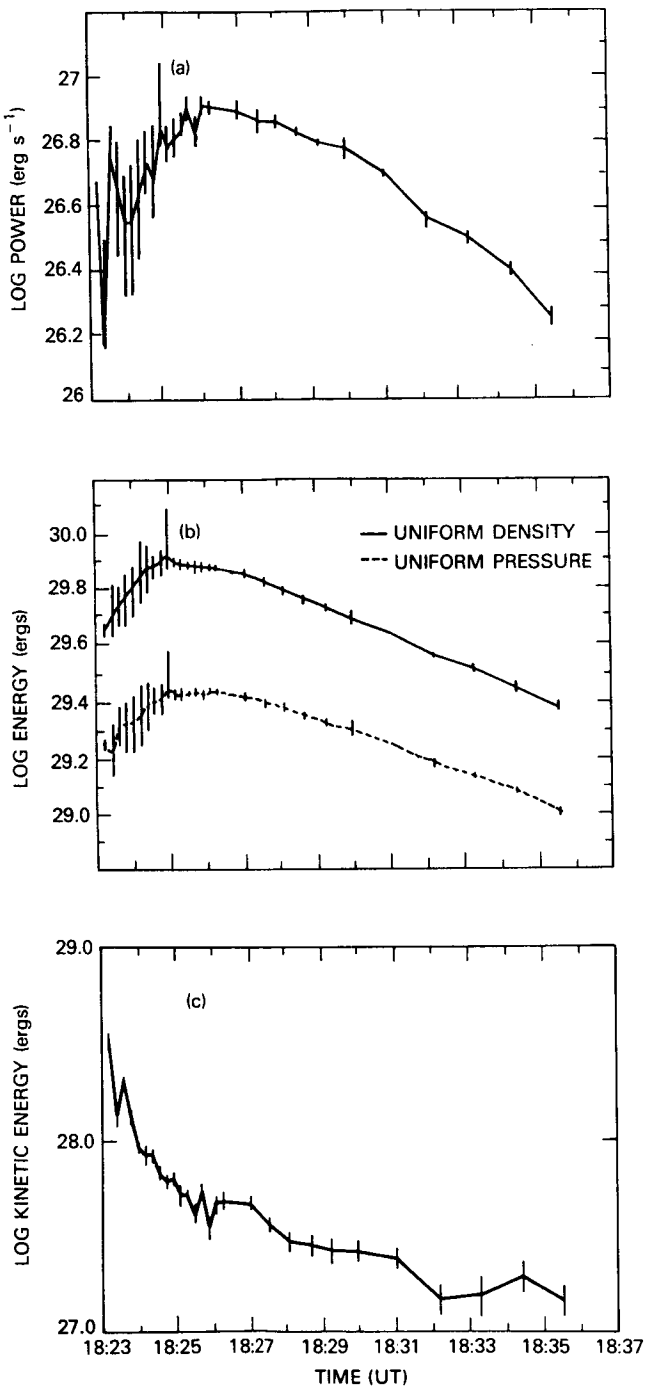

Figure 5.3.8 The radiated power (a), thermal energy (b), and kinetic energy (c) of the soft X-ray emitting plasma as functions of time for the 1980 June 29 flare. These quantities were derived from the BCS and HXIS data. The error bars represent ± 1σ uncertainties. The error bars on the kinetic energy estimates were calculated from the uncertainties of the line widths and electron temperatures but neglect the uncertainties of the estimated volume and emission measures.

5.3.3.4 The 1980 August 31 Flare

The properties of the impulsive double flare on 1980 August 31 were reported by Strong *et al.* (1984). By combining observations of the two events from several of the SMM instruments (XRP, HXIS, HXRBS, and UVSP) as well as radio and optical observatories, they concluded that the second energy release probably occurred in the corona plasma that was hotter and denser than that of the first flare. They inferred that the differences between the two flares resulted from changes in plasma properties brought about by the first energy release. Comparisons of the radio and X-ray data show that the primary energy release site was contiguous (for energetic electrons) with separate, closed magnetic structures. The loops which emitted the radio bursts were at least 10 times longer than those emitting the X-rays. There was no evidence for emerging magnetic flux in this region around the time of the flare; in fact, the field seemed to be decaying rapidly as the two leader spots approached each other. The primary energy release mechanism involved therefore seemed to be magnetic reconnection caused by the "collision" of these structures due to photospheric motions.

The density was determined from the emission measure and source size. The pre-flare temperature of the active region was found to be approximately 2.5×10^6K with an average emission measure of 3×10^{47} cm^{-3}. As there were no distinct structures visible, the volume was derived from the area of the FCS pixel and a typical soft X-ray scale height and was found to be 4×10^{28} cm^3. The mean electron density was therefore 3×10^9 cm^{-3} for the pre-flare active region. Although there were no pre-flare magnetograms, data taken just after this event showed that there was ample free magnetic energy available even after the flares, to supply all the energy observed. Over the previous days, observations of this active region had indicated that the two leading spots (see Section 5A.4) were moving towards one another. Although the velocities were relatively low (of the order of hundreds of meters per second), the energy involved in these photospheric motions must have been large and supplied the stored magnetic energy in the form of sheared magnetic fields.

The highest spatial resolution available on SMM (3 arcsec from UVSP), indicated that the X-ray emitting region in the first flare was 10^{26} cm^3 with an uncertainty of about a factor of 2. The same volume was assumed throughout both flares, as there was no direct measure of the volume for the second flare although the longer timescales of the second flare imply an increased volume.

The multi-thermal analysis covered the extended temperature range from 2×10^6K to 5×10^7K by using six FCS channels, four BCS lines, and the six HXIS fine-field-of-view channels. Figure 5.3.9 shows P_r, E_{th} and E_k as functions of time. The thermal analysis was not possible until the time of the peak of the first flare in soft X-rays as the count rates were low. In calculating E_{th}, a volume of 7.6×10^{25} cm^3

Table 5.3.2 Energy as a Function of Time for the 1980 June 29 Flare

Time (UT)	18:20:40	18:23:28	18:23:54	18:25:00	18:26:00	18:27:18
Thermal Energy (10^{30} ergs)	1.38	3.4	5.5	7.6	7.6	8.3
Energy Deposit rate (10^{27} ergs s^{-1})	1700	2000	26	30	4	2.5
Cutoff energy (keV)	10	12	26	26	26	26

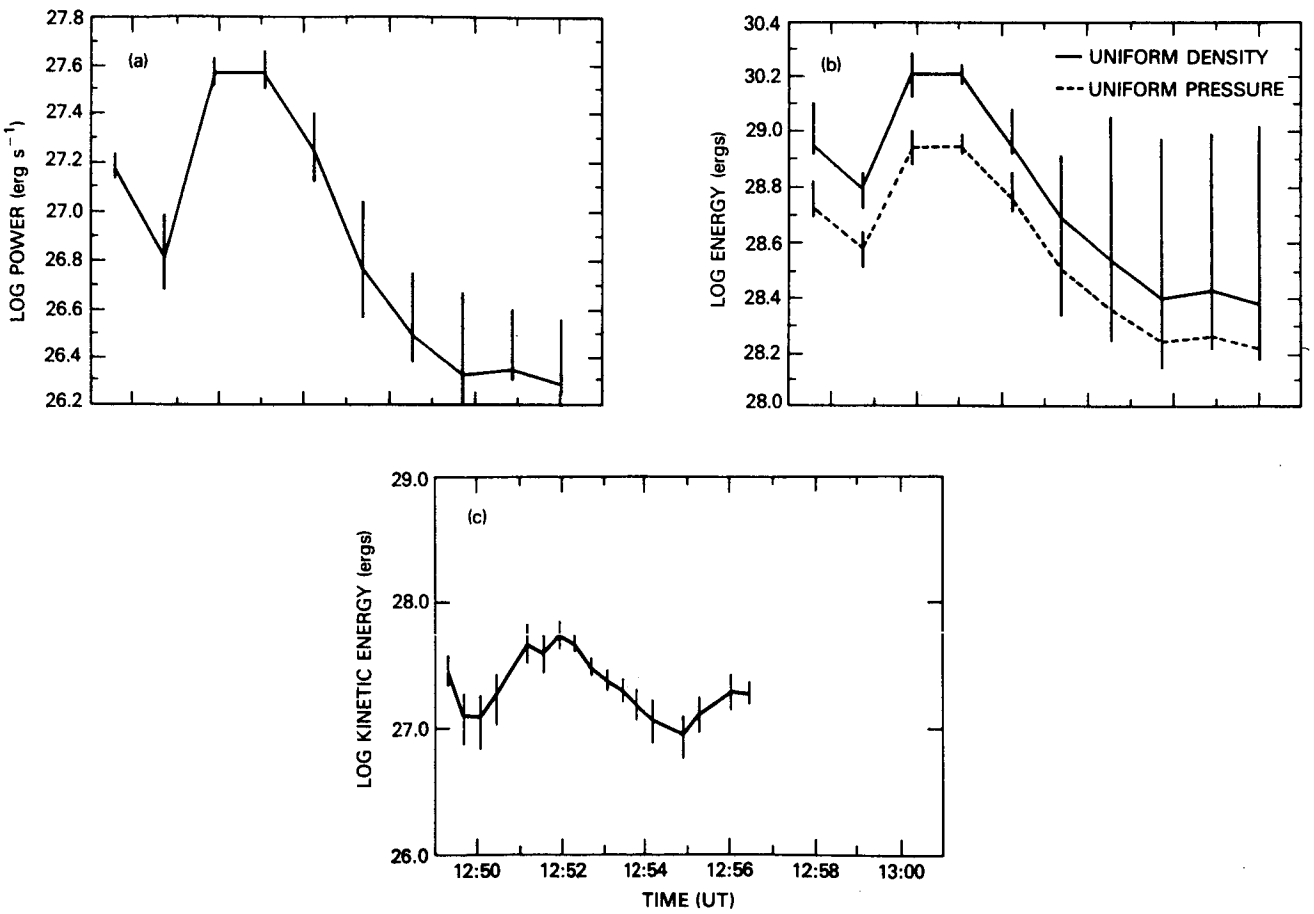

Figure 5.3.9 Same as Figure 5.3.8 for the two flares on 1980 August 31. Compare the peak kinetic energy from the second flare with that of the second flare on 29 June. There is nearly an order of magnitude difference showing that the role of mass motions in this second event are very much inhibited compared to both that of the first flare and the flare on 29 June.

estimated from the HXIS fine-field-of-view images was used for both flares (see Table 5.2.2) even though the volume of the first flare was probably three times larger. The peak value of E_{th} for the second flare was approximately 1.6×10^{29} ergs and compares with a total electron energy of 5×10^{29} ergs.

The energy associated with the turbulent broadening was discussed in Section 5.2.3.4. The peak turbulent energy during the second flare was about 6×10^{27} ergs. It is interesting to note that the ratio of the peak value of E_{th} to the peak turbulent energy for this flare is approximately 27, which compares with 26 for the same ratio for the 1980 June 29 flare. This ratio is close to 10 for the first flare on 1980 August 31.

A comprehensive picture of the mass motions was derived from the BCS X-ray line profiles and from the source motions observed by HXIS. The uncertainties in the velocity measurements are minimal because the flare was compact and therefore not complicated by multiple flare sites. Using the peak integrated DEM and the above volume of 7.6×10^{25} cm^3, we estimated the mass of the "evaporated" plasma and hence the kinetic energy. The potential energy was determined at the peak of the soft X-ray emission from the source size and assuming a semicircular geometry for the loops. Again, by using the density and temperature, we estimated the ionization energy. The results of these calculations are listed in Table 5.3.3 for both flares.

This event illustrates multiple energy release, seemingly a common aspect of flares and a possible reason for so much diversity in flare characteristics. It establishes, for some cases at least, the corona as the locale for the primary energy release involving closed magnetic structures. It also shows that structures of vastly different scale sizes can be involved in the same impulsive release. These are the sorts of morphological boundary conditions which are a prerequisite for continued progress in flare theory.

5.3.3.5 The 1980 November 5 Flare

This was one of the most comprehensively observed flares, with good groundbased data as well as good configurations for the SMM instruments. It was another example of a double flare but with the components separated by more time than for the 1980 August 31 events. The geometry of the flare has been derived by Martens *et al.* (1984), who found the two principal loops observed during the flare to be 1.6×10^9 cm and 7×10^9 cm in length, with a diameter of 1.1 x 10^9 cm. The volume of the larger of the loops was therefore about 4×10^{28} cm^3 if it is assumed to be semicircular.

Using the higher density values from the He-like ion ratios (discussed below), we derived the energetics terms shown in Table 5.3.4. Figure 5.3.10 shows P_r and E_{th} for the two flares on November 5. Estimates of the temperature and emission measure were made from the following parameters: the shape of the FCS soft X-ray light curves (Bornmann 1985a,b), ratios of GOES count rates, DEM fits to the FCS data, satellite-to-resonance line ratios observed with BCS, ratios of HXIS count rates, and thermal fits to HXRBS data. The temperature rose to about 4×10^8K in both flares and fell rapidly during the initial decay, relaxing to a nearly exponential decay late in the decay phase. The emission measure derived from HXRBS reached a maximum of 8×10^{45} cm^{-3} and 10^{47} cm^{-3} for the first and second flare, respectively. The soft X-ray instruments showed emission measures which began and ended near 10^{48} cm^{-3} and reached a maximum value of 3 to 6×10^{49} cm^{-3}.

The electron density estimates during the second flare differ by roughly two orders of magnitude. Duijveman *et*

Table 5.3.3 Non-Thermal Terms of the Energy Budget for the 1980 August 31 Flares

Energy term	Energy in first flare (ergs)	Energy in second flare (ergs)
Kinetic energy		
Turbulence	4×10^{29}	$< 3 \times 10^{27}$
Upflows	5×10^{28}	$< 2 \times 10^{27}$
Translational	7×10^{28}	1×10^{28}
Total	5×10^{29}	1×10^{28}
Potential energy	1×10^{27}	1.5×10^{27}
Ionization potential energy	3×10^{26}	3×10^{26}

Table 5.3.4 Energetics Components in ergs for the 1980 November 5 Flare

Term	Peak	Decay	Total
Radiative losses	3×10^{28}	6.2×10^{26}	2.8×10^{29}
Thermal energy	7×10^{29}	3×10^{27}	
Mass motions (upflows)	4×10^{29}	2×10^{28}	
Mass motions (turbulence)	4×10^{28}		

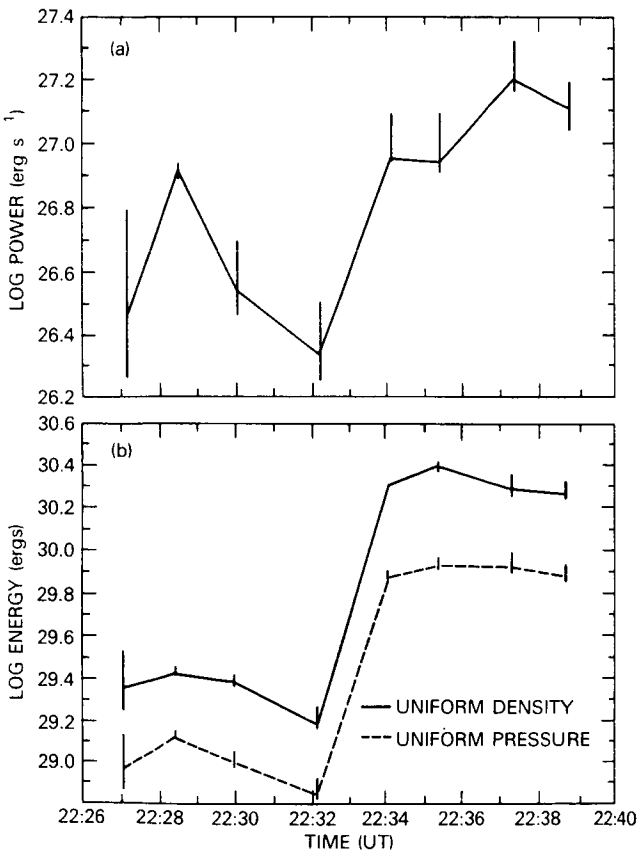

Figure 5.3.10 The evolution of (a) the radiated power (ergs s^{-1}) and (b) the thermal energy (ergs) for the 1980 November 5 flare from combined BCS and HXIS data. The error bars represent ± 1σ uncertainties. These quantities are calculated for the thermal plasma above 10^7 K only.

al. (1982, 1983a) used the emission-measure volume technique, assuming a line-of-sight depth of the emitting region of 6000 km, to find electron densities in the two principal loops of 2.5×10^{10} and 9×10^9 cm^{-3}. Density estimates made from FCS line ratios (Figure 5.3.11) indicate that the density fell from 1.5×10^{12} cm^{-3} at the time of peak soft X-ray flux to 3.0×10^{11} cm^{-3} near the end of the flare decay (Wolfson *et al.*, 1982; Bornmann 1985a). For times when both density estimates are available, the emission-measure volume estimates are a factor of 30-50 lower than

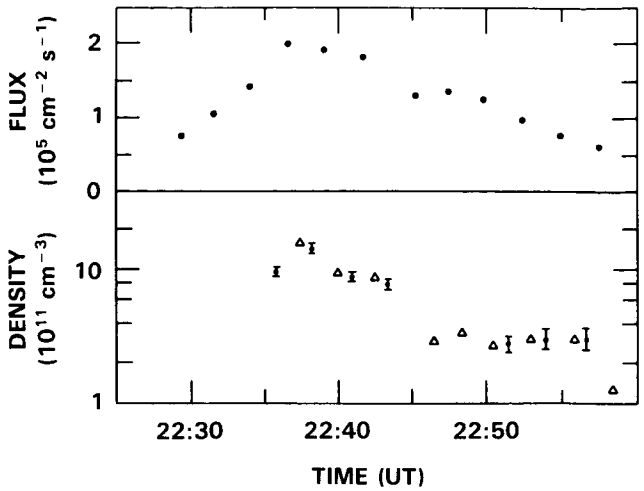

Figure 5.3.11 The evolution of the density and the Ne IX flux during the flare of 1980 November 5. The density is derived from the line ratios of He-like Ne IX (figure courtesy of C.J. Wolfson).

the line ratio estimates. This discrepancy could be the result of emission from separate spatial regions, but this seems unlikely since both detectors sampled overlapping regions in space and energy. Alternatively, the line ratio estimate could be correct if the filling factor was 10^{-3} to 10^{-4}.

However, Wolfson *et al.* (1983) found that the emitting volume observed with FCS decreased from 3×10^{25} to 3×10^{24} cm^3 during the decay of the flare, assuming the temperature remained constant. The volume of an FCS pixel is about 10^{27} cm^3 ($A^{3/2}$), which gives a filling factor of between 3×10^{-3} and 3×10^{-2}. Thus, two separate estimates of the filling factor for this flare both indicate the need for filling factors of the order of 10^{-3}.

DEM analysis following the method of Withbroe *et al.* (1975) and Sylwester *et al.* (1980) using the FCS data indicates a high-temperature component which diminished in magnitude and temperature during the decay phase. A second, low-temperature component remained nearly constant with time. This DEM behavior has been observed in other flares examined by our group (cf. Figure 5.3.1).

Bornmann (1985a,b) used the shape of the FCS light curves to determine the temperature and emission measure during the decay of this flare (Figure 5.3.12). She assumed that the plasma was isothermal and that discrepencies between observed and calculated fluxes (which were less than a factor of 2) were due to incorrect assumptions for detector efficiencies and/or atomic abundances. Although the DEM and light curve analyses both used the same data, they lead to different conclusions because of the manner in which the two techniques respond to possible problems in absolute flux calibrations; the DEM method assumes that the values given are correct, whereas the light curve method assumes that the plasma is isothermal and adjusts these values accordingly.

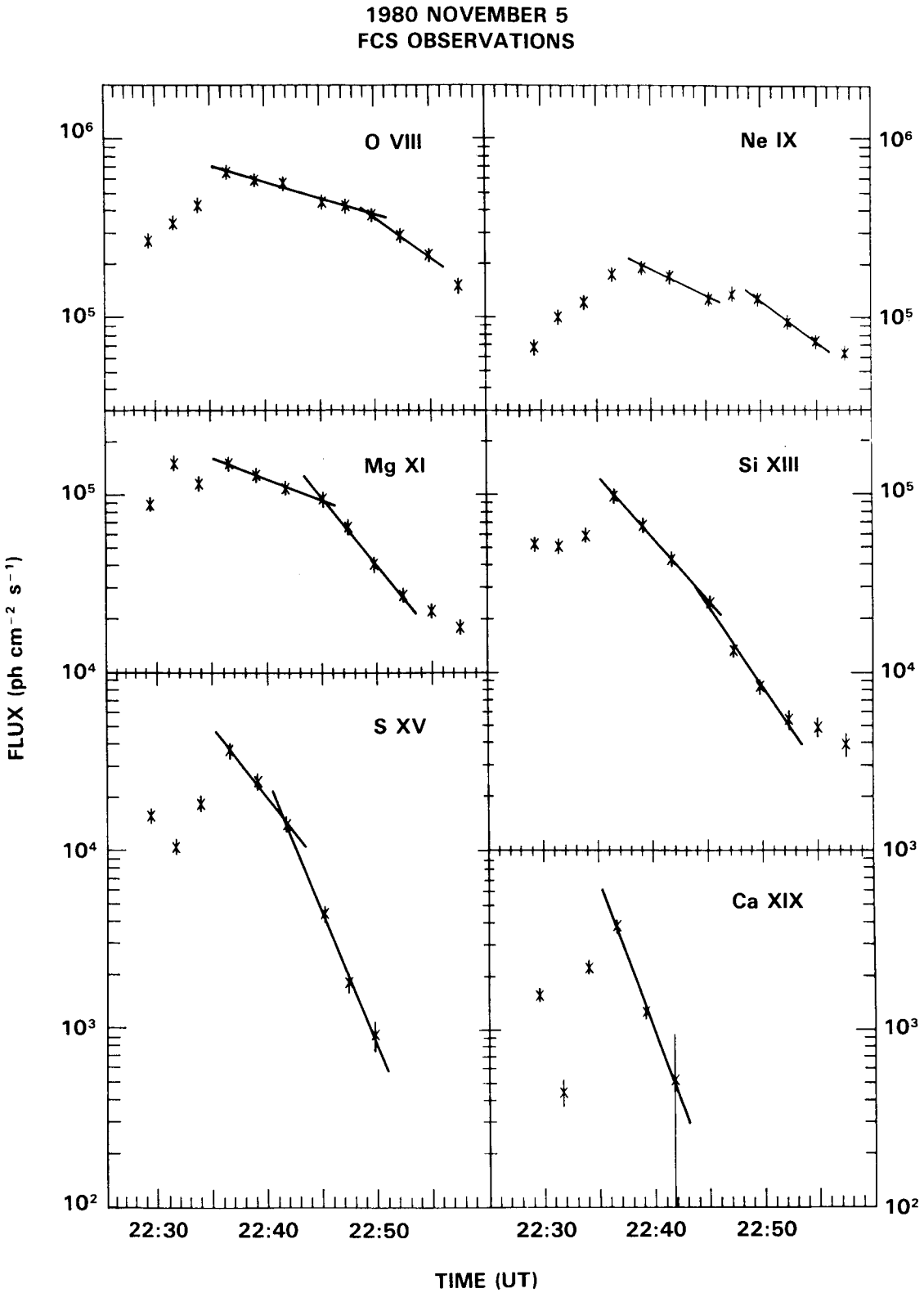

Figure 5.3.12 FCS fluxes for the 1980 November 5 flare illustrating the sharp changes in slope for each of the ions. Note how the ions formed at the higher temperatures have breaks earlier in time.

The total emission measures in both cases agree to a factor of 2. The temperature derived from the light curve lies between the temperatures of the two peaks in the DEM. Further study of these discrepancies is in progress.

The volume derived from the soft X-ray emission measure and electron density (determined from line ratios) was found to increase from 7.2×10^{24} to 3.4×10^{25} cm^3 during the flare decay (Bornmann 1985a). The spatial extent of the flare, as recorded in the lowest-energy HXIS channel (3.5 to 5.5 keV) was not changing during this time, at least on the scale of the 8-arc-sec spatial resoluton. This indicates that the filling factor increased with time during the flare decay. The work done, if the increase in volume is due to expansion of the emitting material rather than to the addition of emitting material in neighboring regions, was $W = \int P\, dV > \int n_e\, k\, T\, dV$, or greater than 3.2×10^{28} ergs (Bornmann 1985a).

Bornmann (1985a) concluded that the mass of the soft X-ray emitting plasma remained constant during the decay phase, although the large errors on this measurement do not eliminate the possibility that the mass varied by a factor of two, reaching a maximum late in the decay phase.

The total radiative loss rate (Nagai 1980, Rosner *et al.*, 1978) for the equivalent isothermal plasma derived from the temperature and emission measure was found to fall from 6.3×10^{26} to 1.9×10^{25} ergs s^{-1} during the decay of the second flare (Bornmann 1985a). The total radiative loss during this period was 2.8×10^{29} ergs.

The total thermal energy ($E_{tot} = n_e\, k\, T\, V$) of the plasma seen in the FCS pixel during the decay of the second flare was 4.2×10^{28} ergs at the time of peak soft X-ray flux, decreasing to 2.2×10^{28} ergs (Bornmann 1985a). Because FCS sampled only a small portion of the flare, the total thermal energy of the entire flare plasma was probably an order of magnitude larger. The thermal energy in the decay phase fell at a rate of 2.7×10^{25} erg s^{-1} (Bornmann 1985b), which is slower than the rate at which energy was lost by radiation. Therefore, additional heating during the decay phase is required.

The energy in mass motions fell off rapidly, at the rate of 1.8×10^{28} ergs s^{-1}. The conversion of the energy in mass motions into the observed radiative and thermal energies could be the source of additional heating, but the rate of decay of the mass motions was too rapid and would require an intermediate storage mechanism before appearing as thermal or radiant energy. The turbulent line broadening began at the same time that the blue shifts appeared and continued for several minutes. The BCS line widths indicate that the turbulent velocities peaked at 100 to 200 km s^{-1}, simultaneously with the hard X-ray peak, and fell essentially to zero during the decay phase. The peak turbulent energy, assuming an electron density of 10^{12} cm^{-3}, was 5.6×10^{27} ergs and fell at the slower rate of 5×10^{25} ergs s^{-1}. If this rate continued past the time at which turbulent broadening was observable, it could account for a significant fraction of the energy lost by radiation.

5.3.4 Flare Modeling

The above studies do not address the problem of the energy source function. Numerical simulations require an energy input function to reproduce the observed fluxes in the coronal lines. By adjusting the input energy profile to agree with the observed evolution of the X-ray line intensities, it should be possible to derive the heating function. The recent rise in interest in numerical simulations of solar flares is dealt with in more detail in Chapter 7. However, that section emphasizes the numerical techniques and differences between the codes. In contrast, the work done for our group by R. Pallavicini, G. Peres and S. Serio used a hydrocode to simulate two real flares.

The 1980 May 7 (15:00 UT) and November 12 (17:00 UT) flares were chosen for this study. In both cases the initial conditions for the models were determined from observations. The one-dimensional, time-dependent fluid equations were solved (see Peres *et al.*, 1982; Pallavicini *et al.*, 1983) subject to Gaussian energy input of the form

$$H = H_0\, f_t \exp[-(s-s_0)^2/(2\,\sigma^2)]. \qquad (5.3.15)$$

In the first stage of the analysis, s_0 was chosen so that the pulse was centered on the loop summit. In other work (Pallavicini *et al.*, 1983; Peres *et al.*, 1984), the fitting has been done for the pulse centered at the base of the loop and for energy deposition with electron beams. However, Pallavicini *et al.* (1983) showed that the exact location of the energy input did not make a significant difference to the global form of the computed light curves. The duration and amplitude of the heating during the rise phase of the flare are obtained by a best fit to the temperature and Fe XXV light curve. This approach is based on the results of Pallavicini *et al.*, who showed that the Fe XXV light curves start to decay as soon as the heating level is decreased.

The May 7 flare was a compact, short-lived event. FCS observations show that it was confined within a single 15 arcsec pixel. An extensive analysis of this event, based on simultaneous SMM and Hα observations, has been given by Acton *et al.* (1982). The flare consisted of a single compact loop with a length (L) of 10^9 cm and cross-sectional area (A) of 9×10^{16} cm^2. The pre-flare temperature at the same location was determined to be $T_e = (2.5 \pm 0.5) \times 10^6$K from the ratio of the intensites of the FCS Ne IX and Mg XI lines. The initial pressure and density have been inferred from the loop temperature and length by using the scaling law of Rosner *et al.* (1978). The derived initial pressure (P_0) was about 10 dynes cm^{-2}, implying a pre-flare coronal density of 10^{10} cm^{-3}.

The parameters and the time evolution function used to fit the observations were $H_0 = 175$ ergs cm^{-3} s^{-1}; $s_o =$

5.7×10^8 cm; $\delta = 10^8$ cm; $f(\tau) = t/150$ for $0 < t < 150$ s and $f(t) = \exp[(150 - t)/\tau]$ for $t > 150$ s.

In the initial model the decay time (τ) was assumed to be zero (i.e., an instantaneous switch-off of the heating function). This allows a good fit to the BCS Ca XIX and Fe XXV light curves during the rise phase of this flare (Figure 5.3.13). The lower-temperature lines from FCS cannot be used to further constrain the fit, as the temporal resolution available during this time was only 155 s. These parameters do not fit either of the BCS lines during the decay phase. The predicted fluxes decay faster than the observed ones. The decay time was increased to accommodate this problem; a value of about 60 s would give very likely the desired result. The large increase in density and temperature in the flare generally causes a decrease in all the characteristic timescales for a given loop model (e.g., the radiative cooling time, the conductive cooling time, and the sound travel time). This imposes a practical limitation on how far the evolution of the flare can be followed into the decay; in this work the model was limited to 20 s after the flare peak.

The thermal energy derived from these models was, typically, an order of magnitude larger than the gravitational and kinetic energies. From the modeling, the energy deposited during the rise phase of this flare was about 3×10^{29} ergs. Allowing for an additional energy deposition during the decay phase with $\tau = 60$ s, the total energy input was 5×10^{29} ergs. The energy deposition would increase if the energy were deposited at the loop footpoints. (For further details see Peres *et al.* (1985)).

The November 12 flare was substantially different from the May 7 flare in that it had a larger spatial extent (covering at least three 15-arc-sec pixels) and a somewhat lower density and pressure in the pre-flare state. For a more detailed description of this flare, see MacNiece *et al.* (1985). The soft X-ray light curves appear to be typical of most flares observed by FCS. Since the raster cadence was faster than for the May 7 flare, the simulations could be carried further.

The flare occurred in a loop with $L = 4 \times 10^9$ cm and $A = 2.5 \times 10^{17}$ cm^2. The pre-flare density and temperature were calculated as above to be 7×10^9 cm^{-3} and 3×10^6K, respectively, corresponding to a P_0 of about 6 dynes cm^{-2}. The heat input was assumed to be at the loop summit (hence s_0 was 2×10^9 cm). The input was assumed to be 10 ergs cm^{-3} s^{-1} at a steady rate for a period of 180 s with a value for s of 5×10^8 cm during the rise phase of the flare. Several values of τ (0, 30, 60, and 140 s) were tried to fit the decay phase. The best fit to the observations was $\tau = 60$ s, which was mainly determined from fitting the Fe XXV light curve, owing to the strong temperature dependence of the emissivity of this line.

Figure 5.3.14 shows a comparison of observations and numerical simulations for the FCS and BCS light curves. The

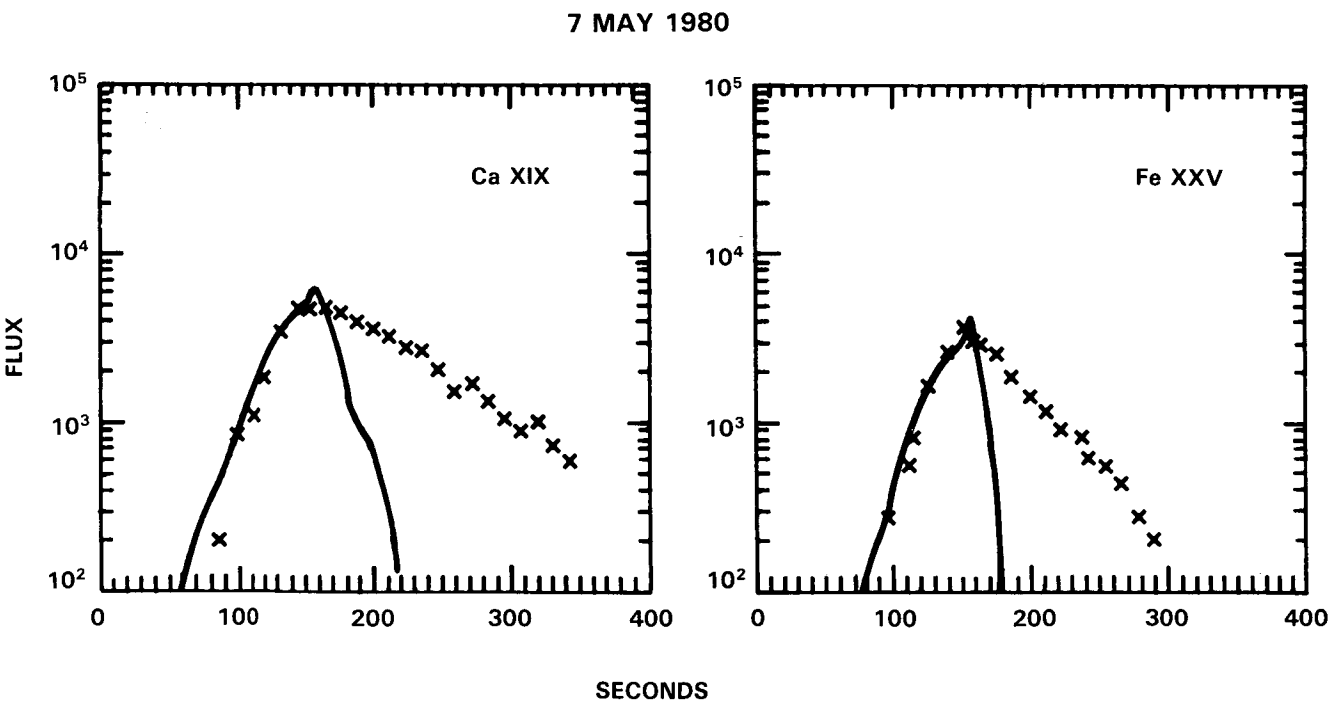

Figure 5.3.13 Predicted light curves (solid lines) from a loop model with an instantaneous switch off of the transient heating at t = 150s, compared to BCS data (crosses) for Ca XIX and Fe XXV (t = 0 corresponds to 14:56:36 UT). The disagreement between observed and predicted light curves in the decay phase indicates that additional heating is required after the peak in Fe XXV.

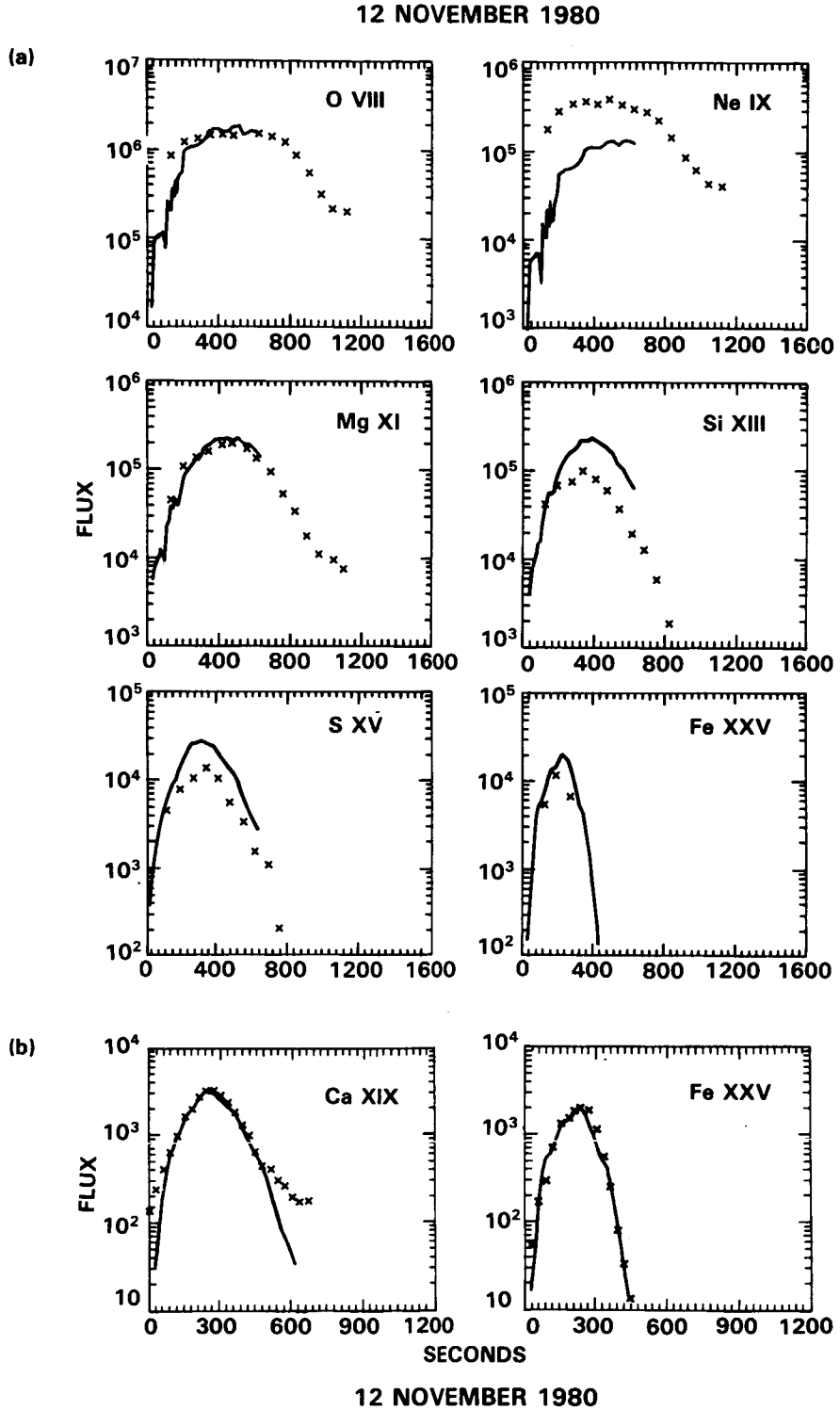

Figure 5.3.14 Comparison of the predicted (solid lines) and observed (crosses) fluxes for the XRP soft X-ray lines in the 1980 November 12 flare. The model has steady heating to t = 180s, followed by an exponential decay with an e-folding time of 60s (t = 0 corresponds to 17:00:00 UT). (a) Comparison for the six FCS channels. (b) Comparison with the BCS lines.

predicted fluxes appear to be in agreement with observation for all lines except Ne IX. Not only is the general time evolution well reproduced, but the absolute flux values also agree with observations within the estimated calibration accuracy. The discrepancy found for Ne IX is not readily explained except in terms of instrumental effects, such as blending with nearby Fe XIX lines and/or crystal fluorescence. Note that the choice of τ = 60 s is made to fit only the Fe XXV light curve.

From the above results, it is possible to evaluate the energy budget of the November 12 flare. Figure 5.3.15 shows E_{th} as a function of time. Again, E_{th} dominated all the other sources of energy by an order of magnitude at any time during the flare. The total energy deposited into the loop for τ = 60 s was 7 × 10^{29} ergs.

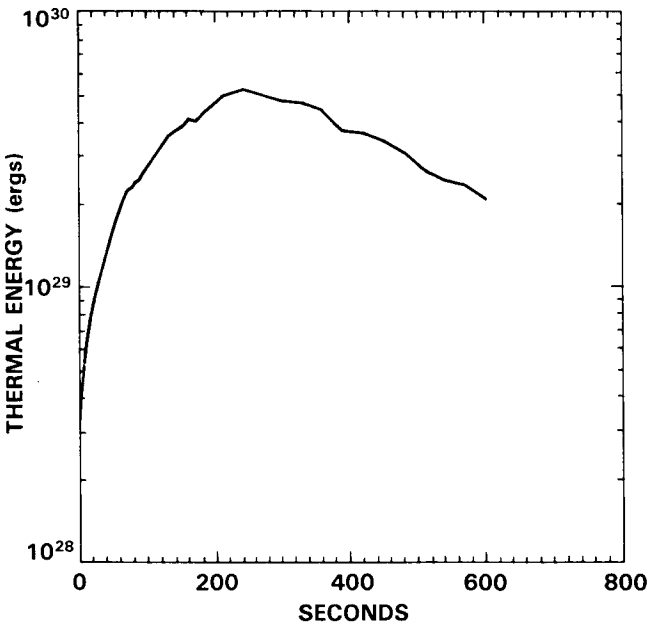

Figure 5.3.15 The evolution of the thermal energy in the 1980 November 5 flare as predicted by the dynamical loop model.

The decay time we have adopted for the heating term has little direct relationship with the decay times of the light curves of the lines of lower ionization stages. In fact, the evolution of the light curves of the "cooler" ion is dominated by the evolution of emission measure and temperature (remember that during evolution, the loop's temperature is hardly uniform). Instead, as soon as the heating is switched off, the Fe XXV radiative efficiency is a very steep function of the temperature up to 70 × 10^6 K (see Figure 8 of Pallavicini *et al.*, 1983). On the other hand, the emission measure of the cooler plasma (say at temperatures near the excitation temperature of O VIII) will keep increasing, essentially because the cooling of the hotter component will enrich the emission measure of the cooler one, if the maximum temperature in the loop is less than 70 × 10^6 K. Therefore, a decay of the Fe XXV line is a good indication of a decay in the heating term, due to steepness of the Fe XXV radiative efficiency.

Actually, the simulations for the November 12 flare, if the heating is switched off abruptly, Fe XXV decays much faster than observed. For this reason we need some smoother decay for the heating. An exponential decay with τ = 60 s gives the best results for Fe. A posteriori, we also see that it gives agreement with the cooler lines, although for these last lines the value of τ, as explained, is less significant. For the May 7 flare light curves, we can infer that τ = 0 does not agree with the observations. The appropriateness of τ = 60 s is only guessed by the shape of the light curves and by our experience of many other simulations.

In summary, if one allows for heating in the decay phase of flares, good agreement with observations can be achieved. The success of this particular modeling effort lies in the fact that a reasonable fit to the form and, in most cases, the amplitude of the light curves of the remaining BCS and FCS lines was obtained, even though the parameters were selected to give a good fit only to the Fe XXV light curve. These results indicate that the bulk properties of the decay phase can be represented quite well by such a fluid model.

5.3.5 Discussion

So far in this section, we have outlined the methods of determining the physical parameters of our five prime flares and have discussed the energy budget at different times during those events. Having determined the temperature, density, and length of the flare loops, we could follow Moore *et al.* (1980) and construct a diagnostic diagram based on the order of magnitude cooling times (Equations 5.3.7-5.3.9) to determine whether our flares require long-term heating. We follow a similar procedure, but first it is important to record the progress that has been made in our theoretical understanding of flare cooling in recent years.

An important physical property of the flare plasma is how the DEM scales with temperature. We find that for 5.5 < $\log(T_e)$ < 7 (Dere and Cook, 1979; Widing and Spicer, 1980; Acton *et al.*, 1983),

$$q = A\, N_e^2\, T\, (dT/ds)^{-1} \approx T^{\zeta}, \qquad (5.3.16)$$

where A is the emitting cross sectional area and ζ is typically 3.5. If we can find a cooling mechanism that gives ζ = 3.5, we may be able to find out how flares cool. Antiochos and Sturrock (1976) considered static conductive cooling in which the downward heat flux is dissipated in the chromosphere, presumably by radiation. They also included a non-uniform magnetic field structure in which the field is stronger at the footpoint of the loop. Underwood *et al.* (1978) found that ζ = 0.5, and for the area change to have significant effect on the cooling time (a factor of about 3), the magnetic field

had to change by a factor of 20 from the loop top to bottom. A refinement of this model was made by Dowdy *et al.* (1983), who considered a variety of flux-tube geometries, and concluded that the shape and amount of divergence were important in determining the magnitude of the inhibition of the heat flux. A slightly different approach to conductive cooling was taken by Van Hoven (1979), who considered the static cooling in a twisted flux tube with constant cross-sectional area and showed that the more the flux tube was twisted, the more the conduction was inhibited. Clearly, twisting gives rise to longer field lines, which makes conduction a less efficient mechanism. However, none of these variations in static conductive cooling makes any change in the form of q. Antiochos and Sturrock (1978) relaxed the static assumption and considered a model in which the chromosphere could respond to a downward heat flux by moving (or evaporating) upward. This model differs in an important way from that in their previous paper (Antiochos and Sturrock 1976), since the thermal energy of the flare plasma is conserved, so that all the energy in the downward heat flux at the base of the model goes into driving an upflow. They found that $\zeta = -0.5$ but noted that no energy is lost in radiation either implicitly or explicitly, so that the effect of evaporation will be overestimated. They did not provide a comparison between static and dynamic cooling. Since the conductive models did not appear to fit the slope of the DEM, Antiochos (1980) then tried radiative models. He found values of ζ between 1 and 2, depending on the form of the loss function chosen. Some of these models include a subsonic downflow, and as an extension to this, Antiochos and Sturrock (1982) included steady-state supersonic downflows driven by a pressure gradient between the loop summit and base. They found that ζ could then take on a value of 3.5 and concluded that the decay of the solar flares involved a large downward velocity at temperatures between 5×10^5 and 10^7K. However, for the flare loop to drain at a reasonable rate (i.e., in a few minutes), they invoked an order-of-magnitude change in the flux tube width from top to bottom. In support of the idea of flare cooling via supersonic downflows, we note that Dere and Cook (1979) have observed large pressure differences between the top and base of a flare loop. However, BCS has not observed obvious red shifts of the order of magnitude required during flare decays. This could be due to a number of factors: the downflowing plasma could be at a lower temperature than BCS can see; and further, it is not an absolute spectrometer and so all the line shifts are relative.

One common feature of the above studies is that large changes in the cross-sectional area of the flux tubes with altitude are invoked. The magnetic field is concentrated in the lower atmosphere to strengths of 1-2 kG (Stenflo 1976). We have only a rough idea of the actual coronal magnetic field strength. Estimates are typically in the range of a few hundred gauss (Schmahl *et al.*, 1982), giving a magnetic divergence of about 3 or 4. It also seems that most of the divergence occurs in the lower atmosphere (Stenflo 1976), i.e., in a region in which the physical validity of the above models is doubtful. It is therefore difficult to accept that flux divergence plays a significant role in the flare cooling process, and so the supersonic cooling model does not seem viable.

Finally, the decay phase of flares has been studied numerically (Antiochos and Krall, 1979; Antiochos, 1980; Nagai, 1980; Doschek *et al.*, 1982; Pallavicini *et al.*, 1983) with similar results. The first four of these papers all obtained large scale, supersonic downflows in the decay phase. The velocity of these flares was typically 50 – 70 km s^{-1}, implying that for them to be supersonic, the temperature had to be less than about 2×10^5 K. It is difficult to see how such flares can explain the slope of the emission curve up to temperatures of 10^7 K. The Pallavicini simulation, although run for long enough, does not discuss the dynamics of such flows. It therefore appears that the physical mechanism responsible for the $T^{3.5}$ slope of the DEM is still unclear. Supersonic downflows seem to come closest to explaining this phenomenon, but the problem of the extremely short draining timescales must be resolved. One potential solution is to relax the fluid approximation, as has been done in quiet-Sun studies by Shoub (1983).

Another problem in studying flare cooling is that of filling factors. As has been stated in Section 5.3.2, the possibility of filling factors of the order of 1% or less means that the electron density can be wrong by an order of magnitude if derived directly from the emission measure and estimated volume. The obvious immediate effect of this is to reduce the radiative cooling time and increase the conductive cooling time by the same factor. This effect can easily be allowed for in the cooling time formulae. However, such an adjustment may be too simplistic. It assumes that any fine structure giving rise to such a small filling factor is composed of long, thin strands which still communicate to the lower atmosphere and still lose energy by conduction, although at a reduced rate. An alternative picture is that the filamentation gives rise to small, isolated regions in the corona that do not communicate with the photosphere and so are unable to lose their energy by conduction. An example of this is the magnetic islands that arise in the tearing mode (Van Hoven, 1981). These small parcels of plasma can then only cool by radiation and so give cooling times inconsistent with the values derived from the equations simply adjusted for the filling factor. Clearly, our understanding of the coronal fine structure during flares will be important in determining the bulk properties of the decay phase of flares. It is worth noting that the three SMM flares (April 8, April 30, and November 5) in which we can compare the density derived from X-ray line ratios with that from the emission-measure volume approach are all large volume flares. An interesting goal for the renewed SMM operations should be to make equivalent observations of a compact flare.

A major source of error is that the behavior of a plasma in a temperature gradient is not well understood. The form of the conductive cooling time derived earlier relies on the Spitzer-Harm (1953, hereafter SH) description of heat conduction, which descibes a plasma only slightly displaced from a Maxwellian. In fact, under not very rigorous circumstances, the SH form of the heat conduction coefficient fails, and in flare plasmas it may fail badly. Rosner *et al.* (1984) have given a concise review of these failings, and we now paraphrase their arguments as applied to flare plasmas. The SH description of heat conduction is valid only if the mean free path (λ) is much smaller than the temperature scale height [L(T)], where the ratio of the two, R, is defined as

$$R = \lambda/L(T) = 10^{10} F_c/(N_e T^{3/2}) << 1. \qquad (5.3.17)$$

The inequality is strong in the sense that if R = 1/30, the SH calculation overestimates the heat flux by a factor of 2 (Bell *et al.*, 1981). In the case where R = 1 (the free-streaming limit), the error is at least a factor 10, and laboratory results suggest that the error may be even larger. For a flare heat flux of 10^{10} ergs cm^{-2} s^{-1} and a density of 10^{12} cm^{-3} at a temperature of 10^6K, i.e. numbers characteristic of the lower corona, we find R = 0.1. Care must be taken in numerical work to check how well the SH method models the heat flux; Craig and Davys (1984) outline a method that involves a gradual reduction of the heat flux as one moves away from the SH regime rather than the sudden jump used by many other authors.

Let us quantify these ideas by considering the five prime flares. Table 5.3.5 shows the principal parameters of each flare. The cooling times due to conduction and radiation with a filling factor of unity have, in some cases, large uncertainties as a result of lack of accurate information about the loop length. The other timescales given in Table 5.3.5 are as follows: τ_{motion}, the time constant of the temperature decay due to enthalpy flux as proposed by Veck *et al.* (1984) and defined by Equation 5.3.9; τ_{drain} (= L/C_s), where C_s is the sound speed, is the time taken for the material to drain from a loop assuming a large pressure gradient and supersonic flows.

First, note that τ_{drain} is much shorter than both τ_{obs} and τ_{motion}. The differences between these timescales is that the former allows for supersonic motions and the latter do not. Thus, the fact that $\tau_{drain} << \tau_{obs}$ suggests that the supersonic downflows postulated by Antiochos and Sturrock (1982) are not present. Consider the loop to be filled with a plasma for which the filling factor is unity and the thermal conduction is described by SH. Then the May 21 and November 5 flares both require long-term energy deposition, since the difference between their calculated and observed cooling times are so significant. The other flares, however, would not appear to require further energy deposition. This is consistent with the predictions of Moore *et al.* (1980).

Table 5.3.5 The Principal Parameters and Timescales of the Prime Flares

Date 1980		Apr 8	May 21	Jun 29	Aug 31	Aug 31	Nov 5
Time (UT)		03:07	21:00	18:21	12:49	12:52	22:33
T_e (10^6K)		8.9	10.0	20.0	12.9	14.8	8.9
n_e ($10^{11}cm^{-3}$)		0.4	1.0	3.5	3.2	3.8	1.4
L (10^9cm)		1.6	3.2	6.3	0.5	0.5	1.6
τ_c	(s)	250	950	2400	50	46	1280
τ_r	(s)	4500	2000	1150	800	750	230
τ_{motion}	(s)	4600	3960	1163	720	600	
τ_{drain}	(s)	67	95	20 - 80	14	13	52
τ_{obs}	(s)	1200	12000	1300	25	45	600

If the filling factor is now set to 0.01 but still with SH, the radiative cooling times decrease by an order of magnitude. Then the May 21 and November 5 flares cool more quickly than before, but the June 29 flare would also require long-term heating, since it cools very effectively by radiation. Neither of the August 31 flares would require any heating, but their cooling is now dominated by radiation rather than by conduction. This is a function of our choice of filling factor, since a filling factor of 0.1 to 0.0001 would make this conclusion more doubtful. However, if thermal conduction is inhibited but the filling factor is 1.0, then the August 31 flares may need long-term heating, whereas the June 29 flare does not.

Even with these simple approximations, the overall picture of flare decay is confusing. All that can be concluded is that if the observed decay time is longer than the radiative cooling time for a filling factor of unity, then long-term energy deposition is required, since any smaller filling factor will simply make the plasma cool more quickly. However, if the flare appears to cool principally by conduction with the right timescale, care must be used since other factors can invalidate this conclusion. One must also be careful when invoking long-term heating, since the need for this can be removed by a combination of physical effects. Peres *et al.* (1984) found that the computed parameters decayed too rapidly when their model was compared with the observations, and so concluded that long-term heating was required. They found a very simple function that reproduced the observed light curves quite well. However, it is equally possible that the extended decay could be caused by a filling factor effect or by a conductive heat flux limitation. We can therefore only conclude that the question of how a flare

plasma cools is less clear than it was before. In reality, our knowledge of the microphysics of plasmas is so poor that we must consider a large number of possible models before making any positive conclusions.

5.3.6 Summary of Conclusions

Let us address the five conclusions of Moore *et al.* (1980) and suggest how future theoretical efforts could clarify them further.

(1) We find that, under the assumption of filling factors equal to one, the densities obtained in these five flares are consistent with those of Moore *et al.* However, the SMM results suggest that the particles are contained within filamentary structures occupying no more than 1% of the observed volume (de Jager *et al.*, 1983; Wolfson *et al.*, 1983). Thus the densities quoted from the Skylab results are too small by at least an order of magnitude. The large uncertainties in the density and possibility of fine structure dictate our response to the remaining four questions.

(2) Depending upon the flare parameters, either conduction or radiation can dominate the cooling process. Mass motions may also play a role in energy transport, a point not considered by Moore *et al.* We therefore disagree with their conclusion that conduction and radiation are generally equally important. For small filling factors, radiative cooling will dominate.

(3) In the May 21 flare, continued heating is needed, confirming the conclusions of Moore *et al.* The understanding of how this heating can occur has improved on the basis of the work by Forbes and Priest (1982, 1983a, b) and Cargill and Priest (1982, 1983), which is discussed in Chapter 1 of this report.

(4) The question of whether compact flares need long-term heating is now open again as a result of the filling factor problem. We do not know what type of filamentary structure exists in such flares. One possible way of heating such flares is via turbulence (Bornmann, 1985c).

(5) The chromospheric evaporation scenario proposed by Moore *et al.* seems to be confirmed by our work on these five flares.

Thus, two of the original conclusions of Moore *et al.* have been unambiguously confirmed by our work. Unfortunately, the SMM data have confused the other three; but they still could be true. A crucial issue for theorists and observers is to determine the nature of the fine structure in flares. This would appear to hold the key to our understanding of the decay phase.

5.4. RELATIONSHIPS AMONG THE PHASES

C.J. Crannell and H.S. Hudson

5.4.1 Introduction

The overall flare process involves phenomena we have characterized as the "impulsive" and "gradual" phases, following the X-ray signature first recognized by Kane (1969). In addition, evidence exists for a pre-flare phase in some flares, and recent SMM data have shown that a post-flare phase, in which extensive and energetically important coronal activity occurs, may also exist. The data to describe the pre-flare and post-flare phases are insufficient to place them properly into an overall picture of the energetics, aside from noting that these phases may indeed be significant from the energetics point of view. In this section, therefore, we review what is presently known and comment about the possible interactions among the flare structures involved.

5.4.2 Relationship Between Impulsive and Gradual Phases

The distinction between the impulsive and gradual phases of a flare was originally made by Kane (1969). The energetics relationship between these phases has been controversial from the beginning, when Kane and Donnelly (1971) showed that the large energy in 10-1030 Å bursts correlated well with the energy inferred for 10 to 100 keV electrons, assuming non-thermal bremsstrahlung as an explanation of the hard X-ray bursts. This was the first real evidence that particle acceleration during the impulsive phase could have energetically significant consequences in the chromosphere, the source of the EUV flashes. We now have far better data with which to examine this question quantitatively, and this subsection deals with the investigation of the energetic relationship between the impulsive and gradual phases.

That the impulsive and gradual emissions are related can be seen in Figures 5.4.1 and 5.4.2, in which the peak counting rates of hard X-ray bursts (Figure 5.4.1) and the total hard X-ray counts (Figure 5.4.2) are plotted versus the peak Ca XIX soft X-ray counting rate. These scatter plots include all events observed with HXRBS and BCS which have both a peak hard X-ray counting rate greater than 100 counts s^{-1} and a peak soft X-ray counting rate greater than 40 counts s^{-1}. The total hard X-ray counts (TOTAL) are better correlated with the peak Ca XIX counting rate (BCS) than is the peak hard X-ray counting rate. This result supports the conclusion of Neupert (1968) that the gradual soft X-ray emission resembles an integral of the impulsive hard X-ray emission.

The significance of these results must be evaluated in view of the Big Flare Syndrome (BFS) identified by Kahler (1982). He found, quite simply, that bigger flares are bigger at all wavelengths. Quantitatively, the BFS is manifest as correlation coefficients of approximately 0.48, with a range of 0.3 to 0.65, between widely diverse parameters. The correlations shown in Figures 5.4.1 and 5.4.2 clearly indicate a closer relationship than would be expected from the BFS.